

CRACK WIDTH MEASUREMENT FOR NON-PLANAR SURFACES BY TRIANGLE MESH ANALYSIS IN CIVIL ENGINEERING MATERIAL TESTING

F. Liebold¹, H.-G. Maas¹, A. A. Heravi²

¹ Institute of Photogrammetry and Remote Sensing, Technische Universität Dresden, Germany -
(frank.liebold, hans-gerd.maas)@tu-dresden.de

² Institute of Construction Materials, Technische Universität Dresden, Germany - ali.a.heravi@tu-dresden.de

Commission II

KEY WORDS: Material Testing, Deformation Measurement, Crack Width Measurement, Triangle Mesh, Non-planar Surface

ABSTRACT:

This publication concentrates on the photogrammetric crack width measurement of crack patterns of concrete probes under impact loading in high-speed stereo image sequences. The presented algorithm works for non-planar specimens with deformations that only appear tangential to the surface and the method is based on triangle mesh analysis. Experiments were conducted with cylindrical specimens with an impact load affecting parallel to the main axis of the cylinder.

1. INTRODUCTION

To reduce damage from impact loading due to natural catastrophes, buildings and walls can be strengthened with material-bonded composites. These composites are analyzed in dynamic tests where photogrammetric deformation measurement techniques are used. High-speed stereo systems offer the possibility to analyze impact tests due to their high temporal resolution. For civil engineers, the detection of cracks and the measurement of the according widths are an interesting issue. In recent years, several publications were contributed in the field of photogrammetric crack width determination. (Dare et al., 2002) applied edge detection techniques such as the Fly-Fisher algorithm and the Route-Finder algorithm to detect cracks in single images of crack patterns and also measured crack widths by the analysis of profiles perpendicular to the crack courses. In (Lange, Benning, 2006), the theoretical crack opening vector is expressed as follows:

$$\vec{t}_c = \begin{pmatrix} \text{crack width} \\ \text{crack edge displacement along the crack course} \\ \text{vertical crack edge displacement} \end{pmatrix} \quad (1)$$

where \vec{t}_c = crack opening vector

This vector bases on the theoretical modes of fracture referring to (Irwin, 1958). (Lange, Benning, 2006) measured artificial targets on concrete specimens with a multi-ocular camera system and computed crack widths with a method given by (Görtz, 2004) using averages of displacements in 4-point-elements, also including the direction of the cracks. However, global rotations between the epochs were neglected. (Barazzetti, Scaioni, 2009) presented a 2D image sequence analysis procedure to determine crack deformations using artificial targets and an orientation frame. (Maas, Hampel, 2006) and (Hampel, Maas, 2009) used digital image correlation techniques to compute a dense displacement field and to analyze crack openings in horizontal and vertical profiles. (Liebold, Maas, 2018) show how to compute crack widths of concrete probes in monocular image sequences using triangle mesh analysis.

Monocular image sequences can only be used for planar surfaces and if the deformations only appear in this plane. The approach presented in this publication gives an extension to the work of (Liebold, Maas, 2018). It will be shown how to detect deformations on non-planar surfaces in triangle meshes between two epochs. Herein, the triangles are transformed into 2D space using the parametrization of a known surface and are analyzed with the 2D algorithm of (Liebold, Maas, 2018). A stereo system is used to measure 3D surface points for each epoch of the sequence. With the mesh analysis of 3D surface points, it is possible to work with non-planar surfaces, for example, from cylindrical specimen. Another advantage of stereo systems is the robustness against relative movements between the object and the camera system. A prerequisite for the algorithm presented here are deformations that are only tangential to the surface (only opening and in-plane shear). Our experiments are designed such that this condition is fulfilled. It is assumed that there is no out-of-plane shear, what means that the z component in Eq. 1 is zero.

The next chapter deals with the description of the experimental setup. In the following part, the method for the crack width determination is presented. After this, the application in the experiment is shown. At the end, a conclusion and an outlook is given.

2. EXPERIMENTAL SETUP

Cylindrical concrete specimens are tested in a gravity-driven split-Hopkinson tension bar to investigate performance of the material at high strain rates (Heravi et al., 2019), see Fig. 1. The height of the specimen is approximately 4 cm.

During the experiment, an image sequence is recorded with a high-speed stereo camera system consisting of two FASTCAM SA-X2 cameras (Fig. 2). The frame rate is set to 100,000 frames per second at an image resolution of 128 × 504 px such that 1 px in image space corresponds to 0.1 mm in object space.

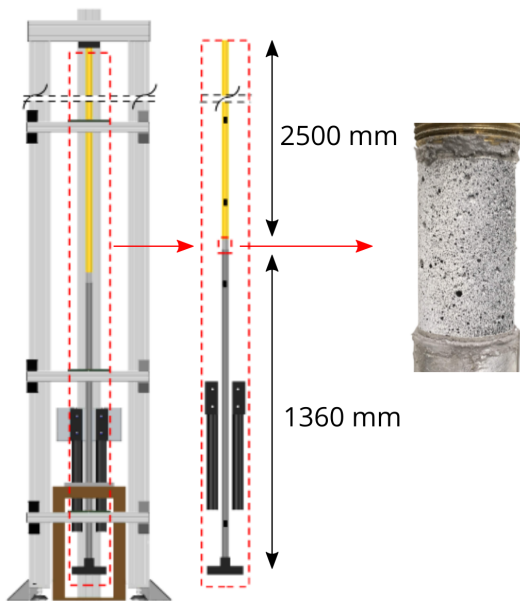


Figure 1. Gravity-driven split-Hopkinson tension bar and cylindrical specimen.



Figure 2. High-speed stereo camera system.

3. CRACK WIDTH MEASUREMENT IN 3D DISPLACEMENT FIELDS

3.1 Preparation and acquisition of the data

First, the inner and the relative orientation of the stereo camera system is determined in a system calibration. Furthermore, the surface of the specimen must have a suitable texture for the matching process. In case of concrete, the surface to be measured may have to be prepared with an artificial pattern. During the experiment, an image sequence is recorded. The first image pair is acquired under zero load without any deformation. The first step of the analysis is the matching of a grid of points between the stereo image pair and between the epochs (current epoch to the reference epoch under zero load). For each epoch, the 3D coordinates are computed by intersection of the corresponding points in the stereo image pair, see Fig. 3.

For each epoch, all 3D points that could be matched successfully in the current time step are triangulated into a mesh using Delaunay triangulation as it is done in (Koschitzki et al., 2011), (Liebold, Maas, 2016) and (Liebold, Maas, 2018), see Fig. 4.

3.2 Workflow of the algorithm

Fig. 5 shows the steps of the presented algorithm for the crack width computation in a flow chart. The single steps of the algorithm are explained in the following sections. The workflow begins after computing the 3D displacements and the triangulation for each epoch.

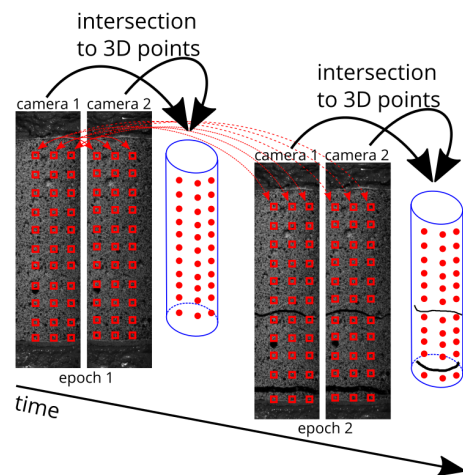


Figure 3. Matching in the stereo image pair and between epochs.

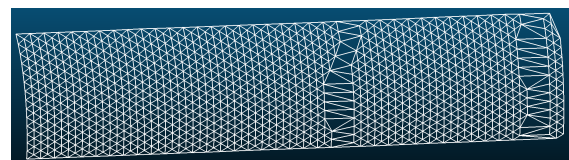


Figure 4. Triangle mesh of the 3D points.

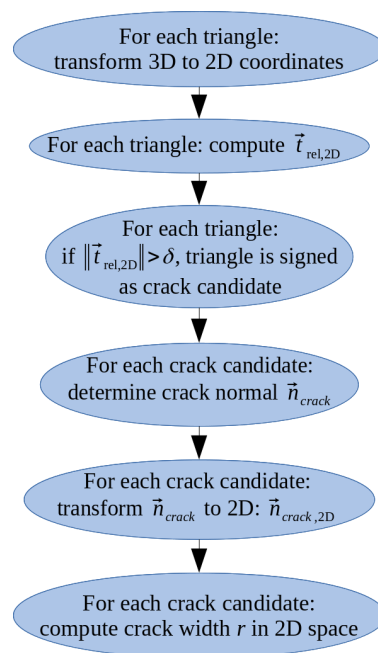


Figure 5. Flow chart of the algorithm: \vec{t}_{rel} is the relative translation vector. δ is a threshold. \vec{n}_{crack} is the crack normal.

3.3 Transformation to 2D

First, the edge vectors between the triangle vertices in the reference (undeformed) and the deformed state are calculated, see Eq. 2. The triangle indices are 1, 2 and 3.

$$\begin{aligned}
 \vec{s}_{12ref} &= \vec{p}_{2ref} - \vec{p}_{1ref} \\
 \vec{s}_{13ref} &= \vec{p}_{3ref} - \vec{p}_{1ref} \\
 \vec{s}_{23ref} &= \vec{p}_{3ref} - \vec{p}_{2ref}
 \end{aligned} \quad (2)$$

where $\vec{s}_{ij,ref}$ = vector from vertex i to j (reference state)

and

$$\begin{aligned}\vec{s}_{12} &= \vec{p}_2 - \vec{p}_1 \\ \vec{s}_{13} &= \vec{p}_3 - \vec{p}_1 \\ \vec{s}_{23} &= \vec{p}_3 - \vec{p}_2\end{aligned}\quad (3)$$

where \vec{s}_{ij} = vector from vertex i to j (deformed state)

The following two terms are computed for the transformation in 2D space for the reference state:

$$\begin{aligned}dx_{13,ref} &= \|\vec{s}_{13,ref}\| \cdot \cos(\angle \vec{s}_{12,ref}, \vec{s}_{13,ref}) \\ &= \frac{\vec{s}_{12,ref}^T \cdot \vec{s}_{13,ref}}{\|\vec{s}_{12,ref}\|} \\ dy_{13,ref} &= \sqrt{\|\vec{s}_{13,ref}\|^2 - dx_{13,ref}^2}\end{aligned}\quad (4)$$

The transformed 2D coordinates in the reference state are:

$$\begin{aligned}\vec{q}_{1,ref} &= (0 \quad 0) \\ \vec{q}_{2,ref} &= (\|\vec{s}_{12,ref}\| \quad 0) \\ \vec{q}_{3,ref} &= (dx_{13,ref} \quad dy_{13,ref})\end{aligned}\quad (5)$$

For the deformed state, the two terms are:

$$\begin{aligned}dx_{13} &= \|\vec{s}_{13}\| \cdot \cos(\angle \vec{s}_{12}, \vec{s}_{13}) = \frac{\vec{s}_{12}^T \cdot \vec{s}_{13}}{\|\vec{s}_{12}\|} \\ dy_{13} &= \sqrt{\|\vec{s}_{13}\|^2 - dx_{13}^2}\end{aligned}\quad (6)$$

The transformed 2D coordinates in the deformed state are:

$$\begin{aligned}\vec{q}_1 &= (0 \quad 0) \\ \vec{q}_2 &= (\|\vec{s}_{12}\| \quad 0) \\ \vec{q}_3 &= (dx_{13} \quad dy_{13})\end{aligned}\quad (7)$$

3.4 Computation of the relative translation vector

In order to compute the relative translation vector in the 2D space, the algorithm from (Liebold, Maas, 2018) is applied using the point triples from Eq. 5 and Eq. 7. Fig. 6 shows the movement of the triangle in 2D. In the deformed state, the upper point has an additional relative translation.

The edge with the minimal distance change is considered as the constant base line edge:

$$b_1, b_2 = i_{min}, j_{min} = \operatorname{argmin}_{i,j} \|\vec{s}_{ij}\| - \|\vec{s}_{ij,ref}\| \quad (8)$$

where b_1 = index of the first base line vertex
 b_2 = index of the second base line vertex

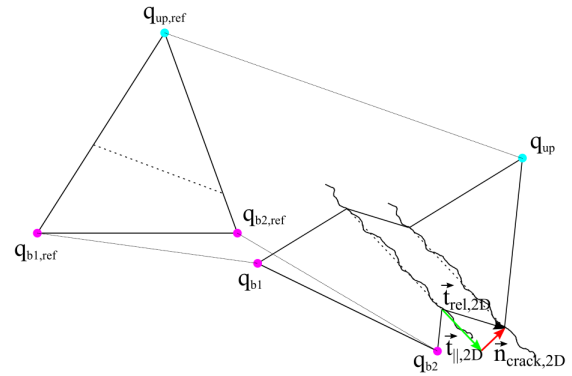


Figure 6. Movement of a triangle crossed by a crack.

For the base line vertices, a Helmert transformation (rigid transformation with fixed scale) is applied:

$$\begin{aligned}\vec{q}_{b1} &= \vec{t}_{2D} + \mathbf{R}_{2D} \cdot \vec{q}_{b1,ref} \\ \vec{q}_{b2} &= \vec{t}_{2D} + \mathbf{R}_{2D} \cdot \vec{q}_{b2,ref}\end{aligned}\quad (9)$$

where \vec{t}_{2D} = translation vector
 \mathbf{R}_{2D} = rotation matrix

The Helmert parameters \vec{t}_{2D} , \mathbf{R}_{2D} can be computed with the coordinates of base line vertices in the reference and the deformed state.

For the upper point, the formula is extended:

$$\vec{q}_{up} = \vec{t}_{2D} + \mathbf{R}_{2D} \cdot \vec{q}_{up,ref} + \vec{t}_{rel,2D} \quad (10)$$

where $\vec{t}_{rel,2D}$ = relative translation vector

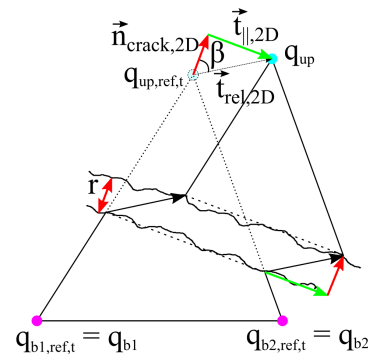


Figure 7. Deformed and transformed reference triangle. r : crack width. $q_{j,ref,t}$: transformed reference points with index j .

The relative translation vector can be computed by reorganizing Eq. 10:

$$\vec{t}_{rel,2D} = \vec{q}_{up} - \vec{t}_{2D} - \mathbf{R}_{2D} \cdot \vec{q}_{up,ref} \quad (11)$$

The norm of the relative translation vector $\|\vec{t}_{rel,2D}\|$ is used to detect deformed triangles including cracks.

If $\|\vec{t}_{rel,2D}\| > \delta$: the triangle is considered as crack candidate where δ is a threshold depending on the quality of the displacement field. The threshold should be in the order of magnitude of the precision of the 3D object coordinates.

3.5 Computation of the crack normal

For each deformed triangle (crack candidate), the deformed triangles of the second order neighborhood (neighbors and neighbors of neighbors) are determined. Neighbor triangles have at least one common vertex with the crack candidate. Then, a line fit through the center points of these triangles is computed in order to determine the line direction \vec{l} , see Fig. 8.

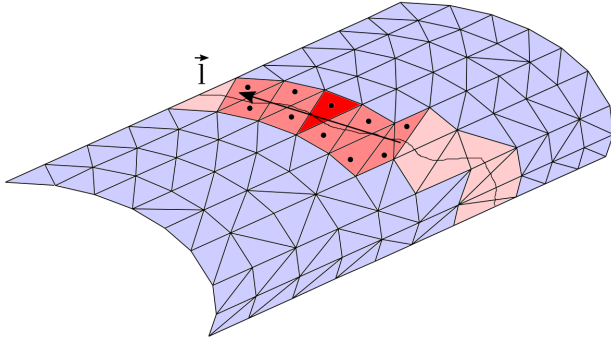


Figure 8. Determination of direction of the crack edge \vec{l} . The triangle with the strong red color is the triangle which \vec{l} is computed for. The center points of the triangle and the deformed neighbor triangles are shown as black points, the deformed neighbor triangles have a less strong red color. The blue triangles are undeformed. The fitted line direction vector \vec{l} is depicted in black.

The normal of the triangle is also needed for the computation of the crack normal in addition to the line direction:

$$\vec{n}_{triangle} = \vec{s}_{12} \times \vec{s}_{13} \quad (12)$$

The crack normal is calculated using the cross product of the normal vector of the triangle and the line direction vector, see Eq. 13 and Fig. 9.

$$\vec{n}_{crack} = \frac{\vec{n}_{triangle} \times \vec{l}}{\|\vec{n}_{triangle} \times \vec{l}\|} \quad (13)$$

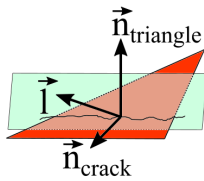


Figure 9. The crack normal is perpendicular to the line direction and the normal of the triangle.

After this, the crack normal is transformed into 2D space. Therefore, the crack normal can be expressed as a linear combination of the edges in the deformed state:

$$\vec{n}_{crack} = v_1 \cdot \vec{s}_{12} + v_2 \cdot \vec{s}_{13} \quad (14)$$

Eq. 14 can be written as a linear system using matrices:

$$\begin{pmatrix} \vec{s}_{12} & \vec{s}_{13} \end{pmatrix} \cdot \begin{pmatrix} v_1 \\ v_2 \end{pmatrix} = \vec{n}_{crack} \quad (15)$$

The system is overdetermined such that the reduced form of the singular value decomposition can be used to solve it:

$$\begin{pmatrix} \vec{s}_{12} & \vec{s}_{13} \end{pmatrix}_{3 \times 2} = \mathbf{U}_0 \cdot \mathbf{S}_0 \cdot \mathbf{V}^T_{2 \times 2} \quad (16)$$

where \mathbf{U}_0 = reduced matrix of the left singular vectors
 \mathbf{S}_0 = reduced matrix of the singular values
 \mathbf{V} = matrix of the right singular vectors

The components v_1 and v_2 can be obtained as follows:

$$\begin{pmatrix} v_1 \\ v_2 \end{pmatrix} = \mathbf{V} \cdot \mathbf{S}_0^{-1} \cdot \mathbf{U}_0^T \cdot \vec{n}_{crack} \quad (17)$$

The reconstruction in the 2D system leads to the transformed 2D crack normal:

$$\vec{n}_{crack,2D} = v_1 \cdot (\vec{q}_2 - \vec{q}_1) + v_2 \cdot (\vec{q}_3 - \vec{q}_1) \quad (18)$$

3.6 Computation of the crack width and the horizontal displacement

The crack width r is calculated by the projection of the relative translation vector (Eq. 11) onto the normal in 2D as shown in (Liebold, Maas, 2018):

$$r = \|\vec{t}_{rel,2D}\| \cdot |\cos\beta| = \frac{\vec{n}_{crack,2D}^T \cdot \vec{t}_{rel,2D}}{\|\vec{n}_{crack,2D}\|} \quad (19)$$

Furthermore, it is possible to compute the shift along the crack (in-plane displacement/shear). The absolute value is:

$$\|t_{||}\| = \sqrt{\|\vec{t}_{rel,2D}\|^2 - r^2} \quad (20)$$

The direction vector in the 2D space without correct orientation (sign) is:

$$\vec{t}_{||,2D,temp} = \begin{pmatrix} -n_{crack,2D,y} \\ n_{crack,2D,x} \end{pmatrix} \quad (21)$$

The correct orientation can be obtained using the dot product to $\vec{t}_{rel,2D}$:

$$\vec{t}_{||,2D} = \begin{cases} \vec{t}_{||,2D,temp} & \text{if } \vec{t}_{rel,2D}^T \cdot \vec{t}_{||,2D,temp} > 0 \\ -\vec{t}_{||,2D,temp} & \text{else} \end{cases} \quad (22)$$

To get the direction in the 3D space, $\vec{t}_{||,2D}$ has to be transformed. First, the system of Eq. 23 has to be solved for \tilde{v}_1 and \tilde{v}_2 . Then, the vector is reconstructed in 3D space and normalized (Eq. 24).

$$\begin{aligned} \vec{t}_{||,2D} &= \tilde{v}_1 \cdot (\vec{q}_2 - \vec{q}_1) + \tilde{v}_2 \cdot (\vec{q}_3 - \vec{q}_1) \\ &= \begin{pmatrix} \vec{q}_2 - \vec{q}_1 & \vec{q}_3 - \vec{q}_1 \end{pmatrix} \cdot \begin{pmatrix} \tilde{v}_1 \\ \tilde{v}_2 \end{pmatrix} \end{aligned} \quad (23)$$

$$\vec{t}_{||} = \frac{\tilde{v}_1 \cdot \vec{s}_{12} + \tilde{v}_2 \cdot \vec{s}_{13}}{\|\tilde{v}_1 \cdot \vec{s}_{12} + \tilde{v}_2 \cdot \vec{s}_{13}\|} \quad (24)$$

4. APPLICATION OF THE CRACK WIDTH DETERMINATION IN THE EXPERIMENT

4.1 Computation of the 3D displacements

The system calibration and the computation of the 3D displacements are done with the commercial software ARAMIS developed by GOM GmbH. The 3D coordinates and displacements serve as input for the application of the crack detection and crack width computation.

4.2 Crack detection and crack width analysis

The algorithm from section 3 is applied on the data. δ is set to 0.02 mm (corresponds to 0.2 px in image space) and defines the threshold for crack candidates.

Fig. 10 shows color-coded maps of the norms of the relative translations of the triangles for the first time steps where deformations could be detected. Therefore, the color-code is very sensitive. The widths are changing in the sequence. After 0.19 ms, the first cracks appear in the visualization. On the far left, there is an area where it is not sure if there is a crack. Later, this possible crack closes as other cracks open. The largest crack at time step of 0.20 ms closes in the following time steps too, whereas the neighbor cracks become larger.

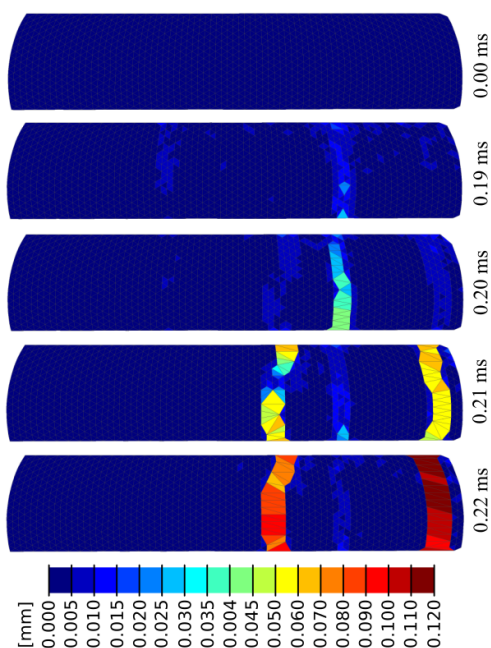


Figure 10. Crack detection. Visualization of $\|\vec{t}_{rel,2D}\|$ for each triangle for some selected time steps at the begin of the crack opening.

Triangles with $\|\vec{t}_{rel,2D}\| > \delta$ can be merged to a region if there are neighbors that also fulfill this condition using region growing, see Fig. 11.

Fig. 12 and Fig. 13 show color-coded visualizations of the norms of the relative translation vectors $\|\vec{t}_{rel,2D}\|$ for two later epochs with 2 cracks. In addition, the histograms of the crack widths of the two crack areas are depicted. In these histograms, some statistical values are given: the mean of the crack widths \bar{r} , the median r_{median} , the maximum crack width r_{max} , the

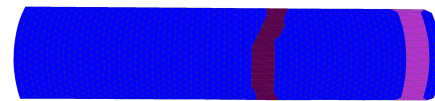


Figure 11. Color-labeled regions of triangles with $\|\vec{t}_{rel,2D}\| > \delta$ at 0.22 ms.

standard deviation of the crack widths σ_r and the standard deviation $\sigma_{r,MAD}$ computed using the median absolute deviation (MAD) which is more robust against outliers.

$$\sigma_{r, mad} = k \cdot median \left(\begin{pmatrix} \|r_1 - median(\vec{r})\| \\ \|r_2 - median(\vec{r})\| \\ \vdots \end{pmatrix} \right) \quad (25)$$

with

$$k = q_{0.75}^{-1} \approx 1.48$$

where

$\sigma_{r, mad}$ = standard deviation computed with MAD

\vec{r} = vector with the measured crack widths

q_p = quantile of order p for $\mathcal{N}(0, 1)$

$\mathcal{N}(0, 1)$ = standard normal distribution

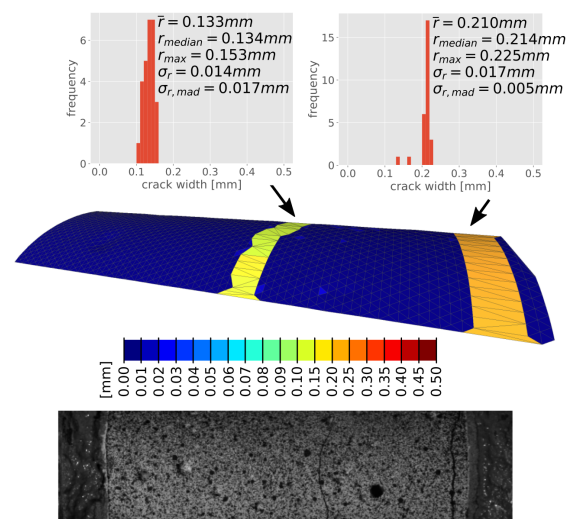


Figure 12. Color-coded visualization of $\|\vec{t}_{rel,2D}\|$ for epoch 25 at 0.24 ms. For the two cracks, histograms of the crack widths are depicted. In addition, the original image of one camera is shown.

In the histograms, some outliers appear due to uncertainties in the normal vector computation at the borders of the mesh. Another reason for outliers are incorrect matching results that are influenced by cracks crossing matching patches. Therefore, in the neighborhood of crack triangles, there are some triangles that are also detected as crack candidates ($\|\vec{t}_{rel,2D}\| > \delta$) but have smaller values of $\|\vec{t}_{rel,2D}\|$.

The diagram in Fig. 14 shows 4 curves: the sum of the mean crack widths of the crack areas ($\sum r_{mean}$), the sum of medians ($\sum r_{median}$) and the sum of the maxima ($\sum r_{max}$). In addition, the total deformation of the sample that is calculated with the wave analysis in the split-Hopkinson tension bar is depicted ($\sum r_{waveanalysis}$) to compare the crack widths with another measurement method. The values of mean and median are strongly depending on the threshold δ which is set to 0.02 mm in this experiment because δ defines which

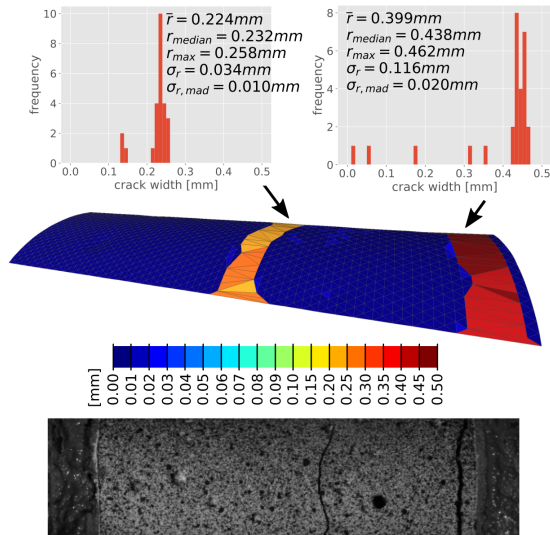


Figure 13. Color-coded visualization of $\|\vec{l}_{rel,2D}\|$ for epoch 29 at 0.28 ms. For the two cracks, histograms of the crack widths are depicted. In addition, the original image of one camera is shown.

triangles are considered as crack candidates. Crack widths according to $\|\vec{l}_{rel,2D}\| \leq \delta$ are not included in the sums ($\sum r_{mean}$, $\sum r_{median}$ and $\sum r_{max}$). Because of that, the values tends to be smaller than the real value and smaller than $\sum r_{waveanalysis}$, too. In this experiment, there are no further external measurements to compare the results of the single crack width computation because it is very difficult to obtain single crack widths with other measurement techniques in high speed tension tests.

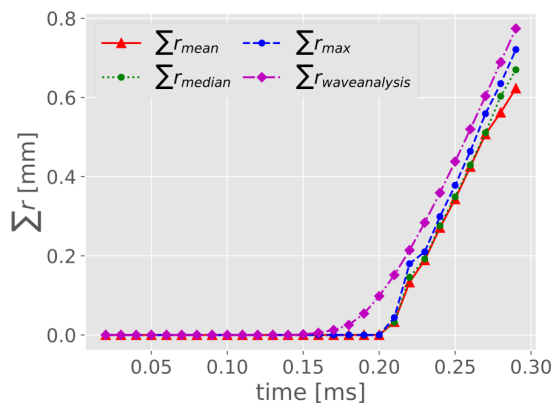


Figure 14. Diagram of the sum of crack widths.

Fig. 15 shows the mean standard deviations $\bar{\sigma}_r$ of the crack widths of each epoch where cracks are detected. Due to outliers, the mean standard deviation computed with the MAD $\bar{\sigma}_{r,MAD}$ is also plotted. $\bar{\sigma}_r$ increases with higher crack widths because the outliers are small (close to δ) and greater values are more influenced by these outliers. In contrast, $\bar{\sigma}_{r,MAD}$ is more or less stable over the time. $\bar{\sigma}_{r,MAD}$ is below 0.015 mm (corresponds to 0.15 px in image space) whereas $\bar{\sigma}_r$ reaches values up to 0.075 mm. Due to the outliers, $\bar{\sigma}_{r,MAD}$ should be preferred as a measure of precision.

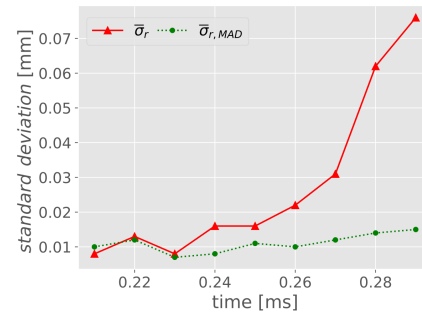


Figure 15. Means of the standard deviations of the crack width areas for each epoch.

5. CONCLUSION AND OUTLOOK

This publication presents a strategy for detection of cracks on concrete specimens with non-planar surfaces in tension tests, and the computation of the according widths. A prerequisite is that deformations only appear tangential to the surface. The accuracy of the crack widths depends on the quality of the displacement field and is in the same order of magnitude. In our experiments, accuracies of approximately 0.01 mm were reached. The next step can be the development of an algorithm that can determine crack opening vectors for cracks with significant z-components. Further improvements should also allow to analyze arbitrary 3D surfaces.

ACKNOWLEDGEMENTS

The research work presented in this publication has been performed within the research training group GRK-2250 at TU Dresden funded by the German Research Council (DFG).

REFERENCES

- Barazzetti, L., Scaioni, M., 2009. Crack measurement: Development, testing and applications of an automatic image-based algorithm. *ISPRS Journal of Photogrammetry and Remote Sensing*, 64, 285–296.
- Dare, P., Hanley, H., Fraser, C., Riedel, B., Niemeier, W., 2002. An Operational Application of Automatic Feature Extraction: The Measurement of Cracks in Concrete Structures. *The Photogrammetric Record*, 17(99), 453–464. <http://dx.doi.org/10.1111/0031-868X.00198>.
- Görtz, S., 2004. Zum Schubrissverhalten von Stahlbeton- und Spannbetonbalken aus Normal- und Hochleistungsbeton. PhD thesis, RWTH Aachen.
- Hampel, U., Maas, H.-G., 2009. Cascaded image analysis for dynamic crack detection in material testing. *ISPRS Journal of Photogrammetry and Remote Sensing*, 64(4), 345–350.
- Heravi, A. A., Curosu, I., Mechtcherine, V., 2019. A gravity-driven split Hopkinson tension bar for investigating quasi-ductile and strain-hardening cement-based composites under tensile impact loading. *Cement and Concrete Composites*, n/a/n/a.
- Irwin, G. R., 1958. *Fracture*. Springer Berlin Heidelberg, Berlin, Heidelberg, 551–590.

Koschitzki, R., Schacht, G., Schneider, D., Marx, S., Maas, H.-G., 2011. Integration of photogrammetry and acoustic emission analysis for assessing concrete structures during loading tests. *Proceedings of SPIE Optical Metrology*, 8085, International Society for Optics and Photonics.

Lange, J., Benning, W., 2006. Crack detection using photogrammetry. *Proceedings of 9th European Conference on Non-Destructive Testing, Berlin*, BB 103-CD, NDT, German Society for Non-Destructive Testing, 1–8.

Liebold, F., Maas, H.-G., 2016. Advanced spatio-temporal filtering techniques for photogrammetric image sequence analysis in civil engineering material testing. *ISPRS Journal of Photogrammetry and Remote Sensing*, 111, 13–21.

Liebold, F., Maas, H.-G., 2018. Sub-pixel accuracy crack width determination on concrete beams in load tests by triangle mesh geometry analysis. *ISPRS Annals of Photogrammetry, Remote Sensing and Spatial Information Sciences*, IV-2, 193–200. <https://www.isprs-ann-photogramm-remote-sens-spatial-inf-sci.net/IV-2/193/2018/>.

Maas, H.-G., Hampel, U., 2006. Photogrammetric Techniques in Civil Engineering Material Testing and Structure Monitoring. *Photogrammetric Engineering and Remote Sensing*, 72(1), 39–45.